Disequilibrating azoarenes by visible-light sensitization under confinement

Julius Gemen[1], Jonathan R. Church[2], Tero-Petri Ruoko[3], Nikita Durandin[3], Michał J. Białek[4], Maren Weißenfels[1], Moran Feller[1], Miri Kazes[1], Magdalena Odaybat[5], Veniamin A. Borin[2], Rishir Kalepu[1], Yael Diskin-Posner[6], Dan Oron[1], Matthew J. Fuchter[5], Arri Priimagi[3], Igor Schapiro[2]*, Rafal Klajn[1]*

[1]Department of Molecular Chemistry and Materials Science, Weizmann Institute of Science, Rehovot 76100, Israel
[2]Fritz Haber Center for Molecular Dynamics Research, Institute of Chemistry, The Hebrew University of Jerusalem, Jerusalem 91904, Israel
[3]Faculty of Engineering and Natural Sciences, Tampere University, P.O. BOX 541, 33101 Tampere, Finland
[4]Department of Chemistry, University of Wrocław, 14 F. Joliot-Curie St, 50383 Wrocław, Poland
[5]Department of Chemistry, Molecular Sciences Research Hub, White City Campus, Imperial College London, 82 Wood Lane, London, UK
[6]Department of Chemical Research Support, Weizmann Institute of Science, Rehovot 76100, Israel

*e-mail: rafal.klajn@weizmann.ac.il, igor.schapiro@mail.huji.ac.il

The process of vision begins with the absorption of light by retinal, which triggers isomerization around a double bond and, consequently, a large conformational change in the surrounding protein opsin[1,2]. However, certain organisms evolved different visual systems[3]; for example, deep-sea fishes employ chlorophyll-like antennas capable of capturing red light and sensitizing the nearby retinal molecule via an energy-transfer process[4,5,6,7]. Similar to retinal, most synthetic photochromic molecules, such as azobenzenes[8,9] and spiropyrans[10,11], switch by double-bond isomerization. However, this reaction typically requires short-wavelength (ultraviolet) light, which severely limits the applicability of these molecules. Here we introduce DisEquilibration by Sensitization under Confinement (DESC) – a supramolecular approach to switch various azoarenes from the *E* isomer to the metastable *Z* isomer using visible light of desired color, including red. DESC relies on a combination of a coordination cage[12] and a photosensitizer (PS), which act together to bind and selectively sensitize *E*-azoarenes. After switching to the *Z* isomer, the azoarene loses its affinity to—and is expelled from—the cage, which can convert additional copies of *E* into *Z*. In this way, the cage·PS complex acts as a light-driven supramolecular machine, converting photon energy into chemical energy in the form of out-of-equilibrium photostationary states, including ones that cannot be accessed via direct photoexcitation.

Azobenzene is arguably the simplest and the most widely investigated photoswitchable compound. The original report on azobenzene[13] dates back to 1834, and its ability to isomerize (*E*→*Z*; Fig. 1a) upon exposure to ultraviolet (UV) light was first reported[14] in 1937. The photoisomerization is accompanied by a large conformational change and a substantial increase in polarity. The metastable *Z* isomer spontaneously relaxes back to *E*; this *Z*→*E* back-isomerization can be accelerated with blue light. Owing to the highly reversible *E*⇄*Z* photoswitching, azobenzene derivatives and other azoarenes have found applications in molecular electronics[15], energy storage systems[16,17], information storage media[18], switchable catalysis[19,20], controlled release[21,22], and photopharmacology[23,24], to name but a few. However, the necessity to rely on UV light to generate the metastable *Z* isomer has severely limited the applicability of these molecules, particularly in biologically relevant applications. Red-shifting *E*-azobenzene's absorption band can be achieved by decorating it with different substituents[25,26,27], but this approach affects the compound's identity, which can compromise its utility in a given application. Meanwhile, supramolecular approaches relying on triplet energy transfer (TET), analogous to those found in living organisms[4], have remained elusive because i) the *Z* isomer of azobenzene is excited to the triplet state preferentially[28] over *E*, and, more importantly,

ii) once generated, the triplet state of azobenzene relaxes preferentially[29,30] (by a factor of >50) to the thermodynamically stable *E* isomer. Therefore, whereas triplet sensitizers can rapidly and efficiently facilitate the equilibration of the high-energy *Z* isomer into the stable *E* state[31,32,33,34], the reverse reaction—i.e., sensitized disequilibration—is far more demanding and has remained unknown.

We hypothesized that such sensitized disequilibration might be achieved using a PS that acts on the *E* isomer of azobenzene with high selectivity. Although the triplet excited state of azobenzene relaxes to the *Z* isomer only occasionally[29,30], a hypothetical *E*-selective PS would not excite *Z* once it is generated; therefore, we expect the repeated action of such a PS on *E*-azobenzene to eventually accumulate a substantial amount of the metastable *Z* state (Fig. 1b). Here, we build on our previous work, where we showed that i) the water-soluble coordination cage **C** (Fig. 1c) binds two molecules of various *E*-azoarenes (which are planar and readily stack on top of each other to form noncovalent homodimers), but only one molecule in the *Z* configuration[35,36] (because of their non-planar geometry), ii) cage **C** can also encapsulate—and thus induce dimerization of—molecules structurally similar to *E*-azobenzene (i.e., planar aromatic molecules), including various dyes[37,38,39], and iii) mixing two different inclusion complexes (each binding two molecules of a given guest), induces a rapid guest exchange between the cages, affording heterodimeric complexes, whereby each cage encapsulates two different guest molecules[40]. Taken together, these observations make us pose the following question: can cage **C** co-encapsulate *E*-azobenzene with a PS while preventing close encounters of the same PS with *Z*-azobenzene?

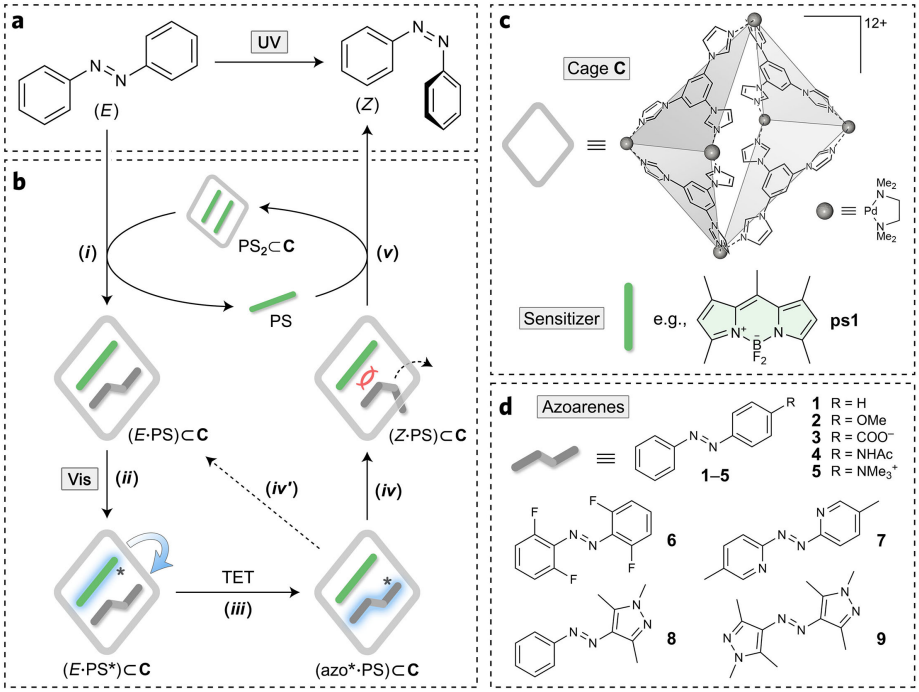

Fig. 1 | The concept of disequilibration by sensitization under confinement (DESC). a, The transformation of the stable *E* isomer of azobenzene to the metastable *Z* isomer traditionally relies on using ultraviolet ($\lambda \approx 350$ nm) light. **b,** The mechanism of DESC: (*i*) Formation of the ternary inclusion complex (*E*·PS)⊂**C** (PS = photosensitizer; **C** = cage); (*ii*) Absorption of a photon of visible light by the PS followed by ISC; (*iii*) Triplet energy transfer (TET) and the formation of triplet-azobenzene, followed by its relaxation (*iv*) to *Z*-azobenzene or, (*iv'*) back to *E*-azobenzene (corresponding to internal conversion); (*v*) Disassembly of the unstable (*Z*·PS)⊂**C** inclusion complex. **c,** Components of the supramolecular system used for DESC: coordination cage **C** and PS (here, BODIPY **ps1**). **d,** Structural formulae of azoarenes **1**–**9** investigated in this study.

The concept of DESC is illustrated in Fig. 1b. The addition of an encapsulated PS (as PS_2⊂**C**) to *E*-azobenzene induces the formation of a ternary complex (*E*·PS)⊂**C** (step *i*). Upon exposure to visible light, PS is promoted to a singlet excited state, which converts into a triplet state via intersystem crossing (ISC) (step *ii*). In step *iii*, PS transfers its triplet energy to the nearby *E*-azobenzene. The resulting triplet azobenzene can either decay to the initial *E* isomer (step *iv′*) or transform into the *Z* state (step *iv*). The former case regenerates (*E*·PS)⊂**C**, which can be re-excited. In contrast, the latter case results in (*Z*·PS)⊂**C**, which is an unstable species since *Z*-azobenzene is too bulky to coexist inside the cage with the PS. Hence, it is expelled from the cage and effectively removed from the equilibrium. Thus, the azobenzene-free inclusion complex of the PS is regenerated (step *v*) and available for transforming additional molecules of *E*- into *Z*-azobenzene.

To verify our hypothesis, we initially focused on the prototypical azobenzene **1** and BODIPY dye **ps1** (Fig. 1c, d). Fig. 2b (dotted brown line) shows the UV/vis absorption spectrum obtained upon mixing aqueous solutions of the respective homodimers—(*E*-**1**)$_2$⊂**C** and (**ps1**)$_2$⊂**C**—in a 1:1 molar ratio. The visible-light region of the spectrum is practically identical to that of pure (**ps1**)$_2$⊂**C** (blue dotted line), indicating a minute fraction of the (*E*-**1**·**ps1**)⊂**C** heterodimer (i.e., the equilibrium shown in Fig. 2a heavily favors the two homodimers). However, exposing this solution to a low-intensity green light (λ = 525 nm, 2.5 mW·cm^{-2}) resulted in a substantial decrease of absorption in the near-UV region (Fig. 2b), indicating the *E*→*Z* isomerization of **1**. This result suggests that the small amount of (*E*-**1**·**ps1**)⊂**C** in equilibrium with the homodimers absorbs green light, whose energy is eventually used to generate the metastable *Z* isomer (Fig. 1b). The low illumination intensities used in our studies exclude the possibility of two-photon isomerization[41,42], which we confirmed directly by power-dependence experiments (Supplementary Fig. 103).

To determine the scope of DESC, we extended our studies to a diverse portfolio of azoarenes, including derivatives with electron-donating and -withdrawing substituents, positively and negatively charged groups, and heterocyclic azoarenes[43] (**2**–**9** in Fig. 1d). All of these compounds were encapsulated as homodimers within cage **C** and, similar to **1**, most of them preferably existed in the E_2⊂**C** form even in the presence of (**ps1**)$_2$⊂**C**. Interestingly, however, azobispyrazole[44] **9** (and, to some extent, azopyrazole[45] **8**) showed a strong tendency to form a heterodimer with **ps1**, as manifested by the intense 509 nm peak in the absorption spectrum (Fig. 2c; dotted brown line). The high fraction of the heterodimer allowed us to grow single crystals and solve its X-ray structure, which shows *E*-**9** and **ps1** bound tightly inside the cavity of **C** (Fig. 2d). Exposure of (*E*-**9**·**ps1**)⊂**C** to 525 nm light quenched its near-UV absorption, consistent with the *E*→*Z* isomerization (Fig. 2c). The putative (*Z*-**9**·**ps1**)⊂**C** heterodimer is unstable, forcing **ps1** into homodimers, which explains why the 400–600 nm part of the spectrum at the end of the reaction is nearly identical to that of pure (**ps1**)$_2$⊂**C** (Fig. 2c). Similar to **1** and **9**, compounds **2**–**8** also switched to their *Z* isomers when exposed to 525 nm light in the presence of (**ps1**)$_2$⊂**C** (Supplementary Fig. 76).

Interestingly, the vastly different heterodimer populations in **1**+**ps1** vs. **9**+**ps1** mixtures do not translate into major differences in the reaction kinetics: the former comprises only ~2% heterodimer but requires only twice as much time as the latter (with a heterodimer fraction of ~80%) to reach a photostationary state (PSS). This finding suggests that the rate-limiting step of DESC is the photoisomerization reaction rather than guest shuttling between the cages, which led us to hypothesize that the process should work efficiently also with catalytic amounts of the PS. Indeed, as shown in Fig. 2e, decreasing the amount of **ps1** to only 0.05 eq with respect to **9** extended the time required to reach the PSS fourfold but did not markedly affect its composition.

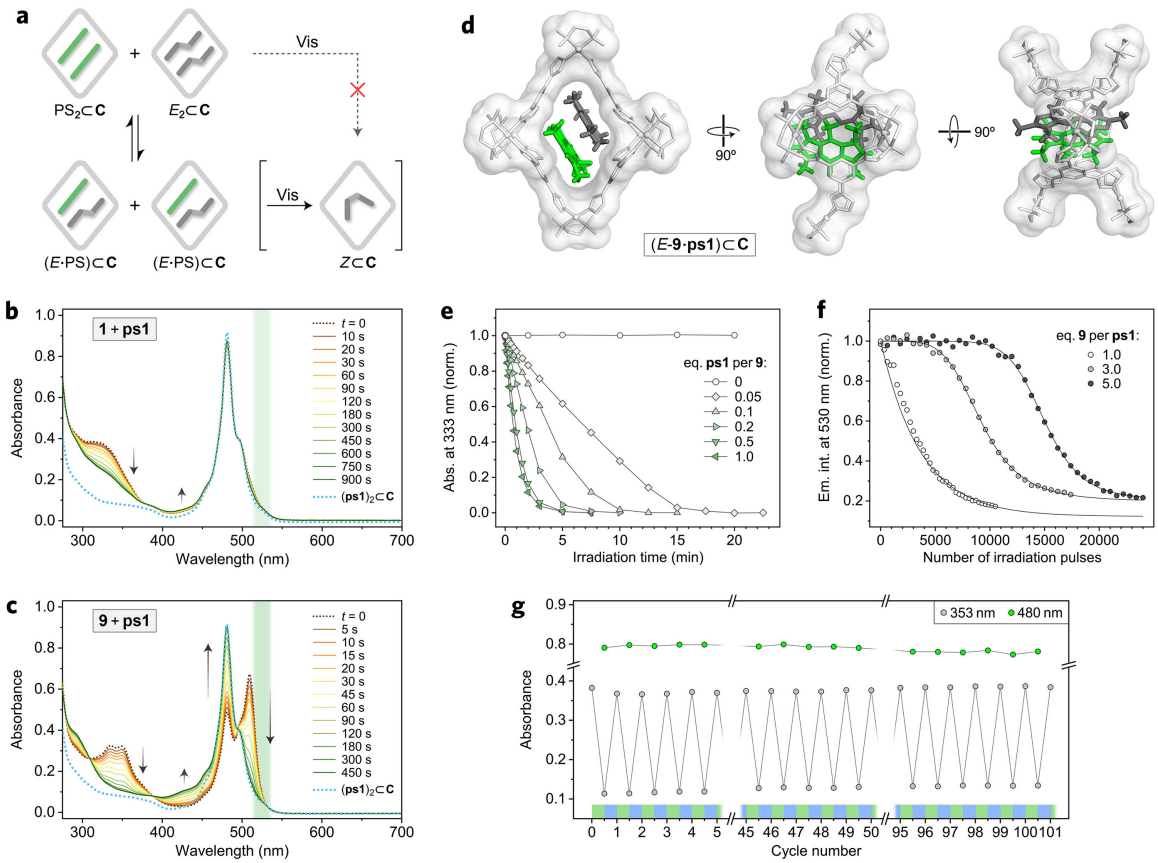

Fig. 2 | Following DESC by steady-state absorption and emission spectroscopy. a, Equilibrium between (*top*) homodimeric inclusion complexes of a PS and an *E*-azoarene (PS_2⊂**C** and E_2⊂**C**, respectively) and (*bottom*) the heterodimeric complex (*E*·PS)⊂**C**. Only *E* residing within the heterodimer—but not the homodimer—can be switched with visible light. The resulting *Z* is encapsulated as a sole guest and cannot be sensitized either. **b,** Absorption spectrum of a 1:1 mixture of (**ps1**)$_2$⊂**C** and (*E*-**1**)$_2$⊂**C** (dotted brown line) and changes in the spectra accompanying irradiation with green light ($\lambda \approx 525$ nm, denoted with green shading). Dotted blue line: absorption spectrum of (**ps1**)$_2$⊂**C**. **c,** Absorption spectrum of a 1:1 mixture of (**ps1**)$_2$⊂**C** and (*E*-**9**)$_2$⊂**C** (dotted brown line; predominantly (*E*-**9**·**ps1**)⊂**C**) and changes in the spectra accompanying irradiation with green light. Dotted blue line: absorption spectrum of (**ps1**)$_2$⊂**C**. **d,** The X-ray crystal structure of the heterodimeric complex (*E*-**9**·**ps1**)⊂**C** (from the left: front view, side view, and top view; light-gray = cage **C**; dark-gray = *E*-**9**; green = **ps1**; water molecules, counterions, and cage protons omitted for clarity). **e,** Following DESC of **9** in the presence of different equivalents of **ps1** (the data were normalized to the 0–1 range, except the experiment with no PS; for raw data, see Supplementary Fig. 73). **f,** Evolution of the emission intensity of **ps1** under 515 nm light (used both to induce DESC and excite fluorescence) as a function of the amount of **9**. **g,** More than 100 cycles of reversible photoisomerization of **9** induced solely by visible light (*E*→*Z*: DESC with 525 nm light for 2 min; *Z*→*E*: direct photoexcitation using 435 nm light for 30 s). The amount of the *E* isomer is proportional to absorbance at 353 nm; the absorption at 480 nm originates from the (**ps1**)$_2$⊂**C** homodimer.

The finding that *E*-**9** and **ps1** form the heterodimer in a near-quantitative yield allowed us to determine the quantum yield (QY) of DESC for this pair. Here, we note that **ps1** within (*E*-**9**·**ps1**)⊂**C** is highly emissive, but its fluorescence with (**ps1**)$_2$⊂**C** is largely quenched[37] – therefore, exposing (*E*-**9**·**ps1**)⊂**C** to a 515 nm pulsed laser led to a gradual decrease of emission (Fig. 2f). When the experiment was repeated in the presence of an extra 2 and 4 eq of (*E*-**9**)$_2$⊂**C**, however, we observed lag periods of ~8 and ~18 min, respectively. The stable fluorescence—despite the ongoing *E*→*Z* isomerization of **9**—indicates that the concentration (*E*-**9**·**ps1**)⊂**C** remains steady, which confirms the rapid exchange kinetics in our system: as soon as the isomerized *Z*-**9** is expelled from the cage, it is replaced by

another copy of *E*-**9** (if available). By assessing the mean number of absorbed photons required to convert the excess of *E*-**9**, we found that each successful *E*→*Z* isomerization event requires 17 photons on average (see Supplementary Section 6 for derivation), which corresponds to a QY of ~6% – a remarkably high value, provided the number of steps separating the excitation of **ps1** from the formation of *Z*-**9** (Fig. 1b).

Once generated via DESC, the *Z* isomer can be back-isomerized to *E* via direct excitation with blue light (435 nm), and the process can be repeated for many cycles. To demonstrate the robustness of DESC, we subjected compound **9** to >100 switching cycles and did not observe any noticeable fatigue: both **9** and **ps1** retained their initial absorbance values (Fig. 2g).

In solution, BODIPY dyes as simple as **ps1** are poor triplet sensitizers[46,47]; therefore, the finding that **ps1** acts as an efficient photosensitizer in DESC is surprising. To obtain mechanistic insights into DESC, we performed transient absorption spectroscopic (TAS) and computational studies (Fig. 3). First, we studied the photoinduced dynamics of the (**ps1**)$_2$⊂**C** homodimer using femtosecond (fs) TAS. Figure 3a shows the fs absorption decays at two different wavelengths, following excitation of (**ps1**)$_2$⊂**C** with a 500 nm laser. The increasing transient absorption at 412 nm at delay times >100 ps, accompanied by the increasing bleach at 483 nm, can be attributed to ISC from the S_1 to the T_1 state. Using microsecond (μs) TAS, we found the resulting triplet state to be remarkably stable, with a monoexponential lifetime of 16.5±0.5 μs under ambient conditions (Supplementary Fig. 109a). As expected from a triplet state, the lifetime is strongly dependent on the amount of oxygen in the solvent; decreasing the amount of O_2 by bubbling N_2 for 4 min and 10 min extended the lifetime of the T_1 state of **ps1** to 160±4 μs and 10.1±0.1 ms, respectively (Supplementary Fig. 109b).

When the fs-TAS experiment was repeated for a 1:2 mixture of (**ps1**)$_2$⊂**C** and (*E*-**9**)$_2$⊂**C** (i.e., a pair with a high tendency to form a heterodimer), the bleach at 483 nm was significantly less pronounced (Fig. 3b, inset), indicating a TET to *E*-**9** (see step *iii* in Fig. 1b). Importantly, the TET and the subsequent formation of *Z*-**9** occur in the ns time regime, i.e., much faster than the lifetime of the **ps1** triplet state, which explains why DESC does not require exclusion of oxygen. In fact, we found the process to be equally efficient in strictly deoxygenated vs. thoroughly oxygenated water (Supplementary Fig. 88).

We also studied the *E*-**9**/**ps1** pair under ambient conditions by μs-TAS (Fig. 3c) and found the intensity of transient absorption at 430 nm immediately after excitation (ΔAbs^{*}_{430}) to be inversely proportional to the amount of (*E*-**9**)$_2$⊂**C**, consistent with the quenching of the **ps1**'s triplet state by its *E*-**9** co-guest via TET. The resulting triplet-**9** can either relax to the initial *E*-**9** isomer or switch to *Z*-**9**, which absorbs at 430 nm – hence the increasing steady-state absorption ($\Delta Abs^{\infty}_{430}$). This intimate relationship between the degree of **ps1** triplet state quenching and the extent of *E*→*Z* isomerization identified by μs-TAS further confirms that DESC proceeds via TET between the **ps1** donor and *E*-**9** acceptor.

To gain further insights into DESC, we studied various azoarene/PS combinations as noncovalent heterodimers using quantum chemical simulations. We consistently found that the lowest-energy triplet state (T_1) within these heterodimers is localized on the PS and the second-lowest triplet state (T_2) is localized on the azoarene, indicating that the PS→azoarene TET is an endothermic process[32,48] (e.g., see Fig. 3d for the energy diagram of **1**·**ps1**). These results led us to hypothesize that the experimentally observed TET might be facilitated by thermal fluctuations of molecules, as suggested previously for other triplet donor–acceptor pairs[32,34,49,50]. Therefore, we studied the variation of the **1**·**ps1** excited state energies on the C–N=N–C dihedral angle (Φ) in azobenzene **1** (which is significantly more flexible than **ps1**). Figure 3e shows a relaxed scan for the **1**·**ps1** heterodimer, demonstrating that an 18º twist in Φ is sufficient to invert the energetic order of T_1 and T_2, making TET energetically favorable. We separately studied the dynamics of the (**1**·**ps1**)⊂**C** heterodimer by multiscale MD simulations (Supplementary Movie 1); these simulations reveal that thermal fluctuations readily allow **1** to adapt conformations with $\Delta\Phi \geq 18º$ at room temperature.

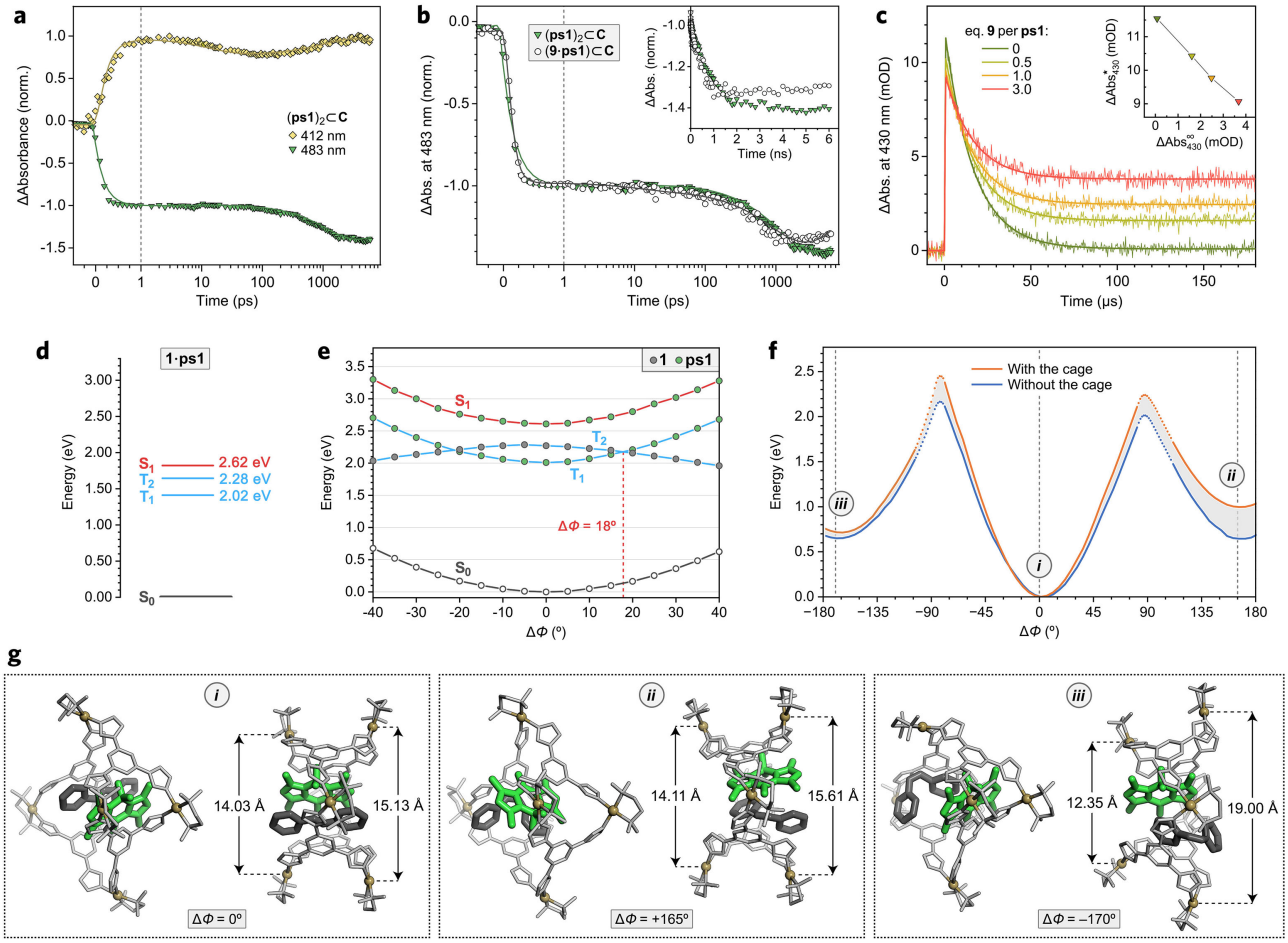

Fig. 3 | Time-resolved spectroscopic (TAS) and computational studies of DESC. a, Normalized decays of fs transient absorption of **ps1** at 412 nm and 483 nm within the (**ps1**)$_2$⊂**C** homodimer (λ_{exc} = 500 nm). Markers: raw data; lines: four-exponential fits. **b,** Normalized transient absorption decays of **ps1** at 483 nm (λ_{exc} = 500 nm) in (**ps1**)$_2$⊂**C** vs. the (*E*-**9**·**ps1**)⊂**C** heterodimer (linear scale in the 0–1 ps time range; logarithmic scale beyond 1 ps). Inset: the same data plotted on the linear scale. **c,** Decays of μs transient absorption at 430 nm (λ_{exc} = 510 nm) in (**ps1**)$_2$⊂**C** in the presence of increasing amounts of (*E*-**9**)$_2$⊂**C**. The thin and thick lines correspond to experimental data and biexponential fits, respectively. Inset: the inverse correlation between ΔAbs^{*}_{430} (absorbance at 430 nm immediately after photoexcitation) and $\Delta Abs^{\infty}_{430}$ (steady-state absorbance). All the TAS results presented here were collected under ambient (non-deoxygenated) conditions. **d,** The energies of the S_1, T_1, and T_2 states in the *E*-**1**·**ps1** heterodimer (the T_1 and T_2 states are localized on **ps1** and *E*-**1**, respectively). **e,** Ground-state relaxed scan along the C–N=N–C dihedral angle Φ in **1** within the **1**·**ps1** heterodimer. The black, red, and blue lines denote the ground state, the bright singlet state, and the two lowest triplet states, respectively. The green and gray markers correspond to the localization of the excited state on the donor (**ps1**) and acceptor (**1**), respectively. **f,** Ground-state relaxed scan of Φ in **1** within the (**1**·**ps1**)⊂**C** heterodimer (orange trace). The blue trace shows the energies corresponding to the same configurations of **1** and **ps1** after removing the cage and its interactions. The scan was performed at the QM/QM2 hybrid scheme. **g,** Optimized geometries of (**1**·**ps1**)⊂**C** for the three $\Delta\Phi$ values indicated in panel **f** (*left:* side views; *right:* top views). The distances between the indicated equatorial Pd nodes describe the degree of cage deformation; the larger the difference between the two Pd–Pd distances, the greater the transition of **C** from a tube-like conformation into a bowl-like conformation. The heterodimer structures (e–g) were optimized using B3LYP-D3/Def2-SVP, the excitation energies (d, e) were calculated at the SCS-ADC(2)//B3LYP-D3/Def2-SVP level of theory, and the cage and nitrate counterions (f, g) were treated using the semiempirical XTB1 method.

We also performed QM/QM2 simulations to better understand the relative instability of the (*Z*·PS)⊂**C** heterodimers vs. (*E*·PS)⊂**C** (see Fig. 1b), which lies at the heart of efficient DESC. The starting point of the simulations was

(*E*-**1**·**ps1**)⊂**C** with a perfectly planar geometry of *E*-**1** (*Φ* = 180º). We performed a relaxed scan by changing *Φ* in steps of 5º in both senses of rotation; the resulting energies are plotted in Fig. 3f in orange. The blue data in Fig. 3f correspond to the same geometries while neglecting the cage and its interactions; therefore, the energetic difference between the two curves (highlighted as gray shading) quantifies the instability of the inclusion complex. We found that rotating *Φ* in one direction affords a highly unstable supramolecular architecture *ii* (Fig. 3g, *center*) that is ~0.35 eV (~8 kcal/mol) higher in energy than free *Z*-**1**·**ps1** (Fig. 3f). Interestingly, rotating *Φ* in the opposite direction gave rise to a geometry where the cage did not markedly increase the energy (*iii* in Fig. 3f and g). However, in this structure, the cage assumes a bowl-like conformation, and *Z*-**1** extrudes from the cavity, facilitating its expulsion to the solution (Supplementary Movies 3–6). The large conformational changes exhibited by the flexible cage **C** during the process are reminiscent of the structural dynamics of enzymes during catalysis[51].

Encouraged by the unexpected sensitization potency of **ps1** under confinement, we considered DESC with other, more red-shifted dyes, including ones not previously known to act as triplet sensitizers. To this end, we first focused on the fluorinated BODIPY **ps2** (Fig. 4a), whose absorption peak is centered at ~553 nm[52] (compared with 499 nm for **ps1**). Interestingly, we found that **ps2** exhibited a higher-than-**ps1** tendency to form heterodimers with various azoarenes; the increased PS–azoarene interactions should further promote DESC. Indeed, Fig. 4b shows that **ps2** induces a near-quantitative *E*→*Z* conversion of an equimolar amount of azobenzene **4** within only 90 s of low-intensity (2.5 mW·cm^{-2}) yellow light (561 nm) irradiation. Moreover, the more efficient DESC allowed us to decrease the PS loading further: at only 0.01 eq of **ps2** with respect to **4**, the PSS was reached within ~20 min (Fig. 4c).

In general, **ps2** is a more efficient DESC agent than **ps1**. However, we found one exception: **ps2** proved unable to induce the switching of azobispyrazole *E*-**9**. To understand this result, we resorted to quantum chemical simulations (see Supplementary Section 8.1) and found the T_1–T_2 energy gap for the *E*-**9**·**ps2** heterodimer to be exceptionally high (1.03 eV; compared to 0.26 eV for *E*-**1**·**ps1** in Fig. 3d). Moreover, relaxed scans analogous to those in Fig. 3e revealed that *Φ* in **9** must twist by 38º—a prohibitively large distortion—for the energies of these two triplet states to cross (Supplementary Fig. 117d). These computational results not only rationalize the experimental findings but provide further (although indirect) support for the involvement of the TET mechanism in our system.

We also worked with resorufin **ps3** and resazurin **ps4** (Fig. 4a), both previously reported to form inclusion complexes of the PS_2⊂**C** type[38]. These two dyes are red-shifted even further; for example, the absorption maxima of the respective heterodimers with *E*-**1** appear at 587 nm and 616 nm, with absorption expanding into the red spectral range. To our satisfaction, exciting the absorption bands on these heterodimers with orange and red light, respectively, resulted in a highly efficient *E*→*Z* isomerization of nearly all azoarene/PS combinations (Fig. 4d–f and Supplementary Figs. 92 and 96).

The performance of DESC is showcased in Fig. 5a, which lists the PSS compositions (blue font) for all the nine model azoarenes shown in Fig. 1d (encapsulated within **C** in water with 0.05 eq of the selected sensitizer; **ps2** for **1**–**7** and **ps1** for **8** and **9**). The reactions were performed on the NMR scale (i.e., milligram quantities of **1**–**9**) and can readily be upscaled to obtain the *Z* isomers on the preparative scale. As control experiments (red font), we irradiated **1**–**9** under the same conditions and in the presence of the PS but without cage **C** (hence, in an organic solvent). In the absence of **C**, the *E* isomers could not be co-confined with the PS, which resulted in negligible amounts of the *Z* isomer via direct photoexcitation (only azobenzene **6**, known for its visible-light-responsiveness[26], afforded a sizeable (14%) amount of *Z*). We note that the positively charged azobenzene[53] **5** (often recognized as a prototypical photopharmacophore[24,54]) showed a particularly impressive contrast in behavior between the presence and absence of the cage, giving rise to 98% of *Z*. Notably, such a *Z*-rich PSS cannot be achieved by direct photoisomerization (of neither (*E*-**5**)$_2$⊂**C** or free **5**) with any wavelength of light (the same is true for compounds **1**, **3**, and **6**) because of the partial overlap of the absorption bands of the two isomers[55]. In contrast, the PSS

composition in our system is dictated by the tendency of the two isomers to form the ternary (azo·PS)⊂**C** complex, and this tendency is much higher for the *E* isomer.

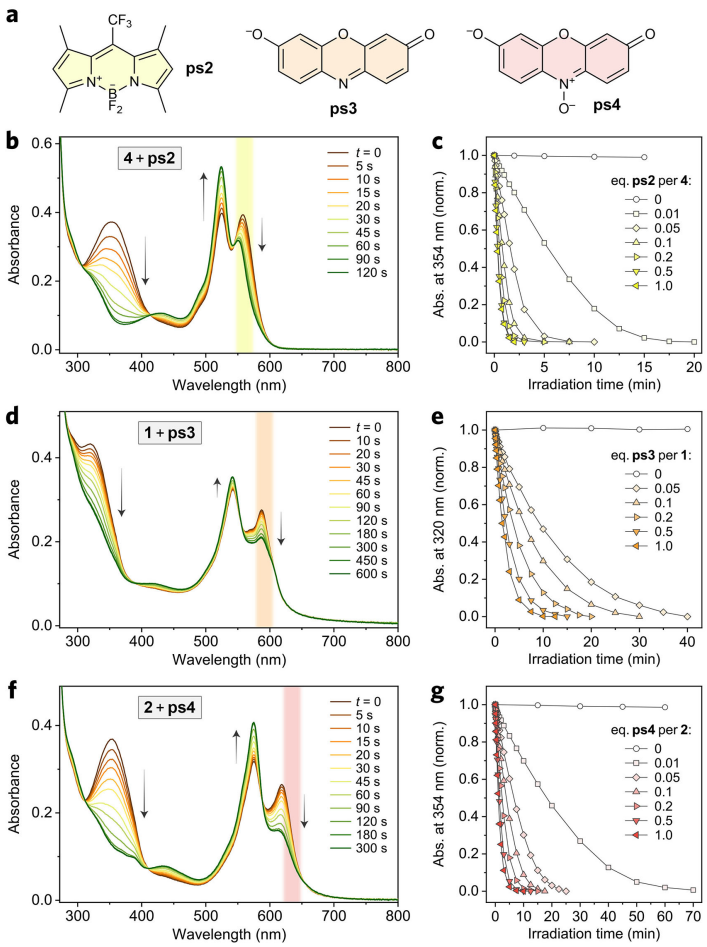

Fig. 4 | Extending the concept of DESC to red-shifted photosensitizers. a, Structural formulae of fluorinated BODIPY **ps2**, resorufin **ps3**, and resazurin **ps4**. **b,** Changes in the absorption spectra of encapsulated **4** in the presence of an equimolar amount of encapsulated sensitizer **ps2** under yellow light ($\lambda \approx 561$ nm, 2.5 mW·cm^{-2}). **c,** DESC (here, for **4**) in the presence of substoichiometric amounts of **ps2**. **d,** Changes in the absorption spectra of encapsulated **1** in the presence of an equimolar quantity of encapsulated sensitizer **ps3** under orange light ($\lambda \approx 599$ nm, 0.8 mW·cm^{-2}). **e,** DESC (here, for **1**) in the presence of substoichiometric amounts of **ps3**. **f,** Changes in the absorption spectra of encapsulated **2** in the presence of an equimolar quantity of encapsulated sensitizer **ps4** under red light ($\lambda \approx 635$ nm at 3.4 mW·cm^{-2}). **g,** DESC (here, for **2**) in the presence of substoichiometric amounts of **ps4**. The data in c, e, and g were normalized to the 0–1 range, except for the experiments with no PS; for raw data, see Supplementary Figs. 82, 90, and 94.

Having demonstrated that the positively charged *E*-**5** can be successfully transformed into *Z*-**5** despite its low affinity to the like-charged **C**, we speculated that other water-soluble azobenzenes may also be efficiently disequilibrated using a substoichiometric amount of not only the PS but also the cage. Figure 5b shows the result of an experiment in which an aqueous solution of the negatively charged **3** was exposed to red light in the presence of 0.005 eq of (**ps4**)$_2$⊂**C**. The absorption spectrum of this solution is dominated by *E*-**3**'s intense absorption peak in the near-UV region; the minute amount of the sensitizer appears as a weak band at ~600 nm (Fig. 5b). Remarkably, exciting this band with low-intensity 635 nm light resulted in a near-complete disappearance of the much more prominent peak originating from another species (*E*-**3**). We found that the PSS contained 88% of *Z*-**3**

(vs. ~0% in the absence of either **C** or **ps4**; Supplementary Fig. 98), indicating that each cage hosted at least 180 *E*→*Z* isomerization events on average.

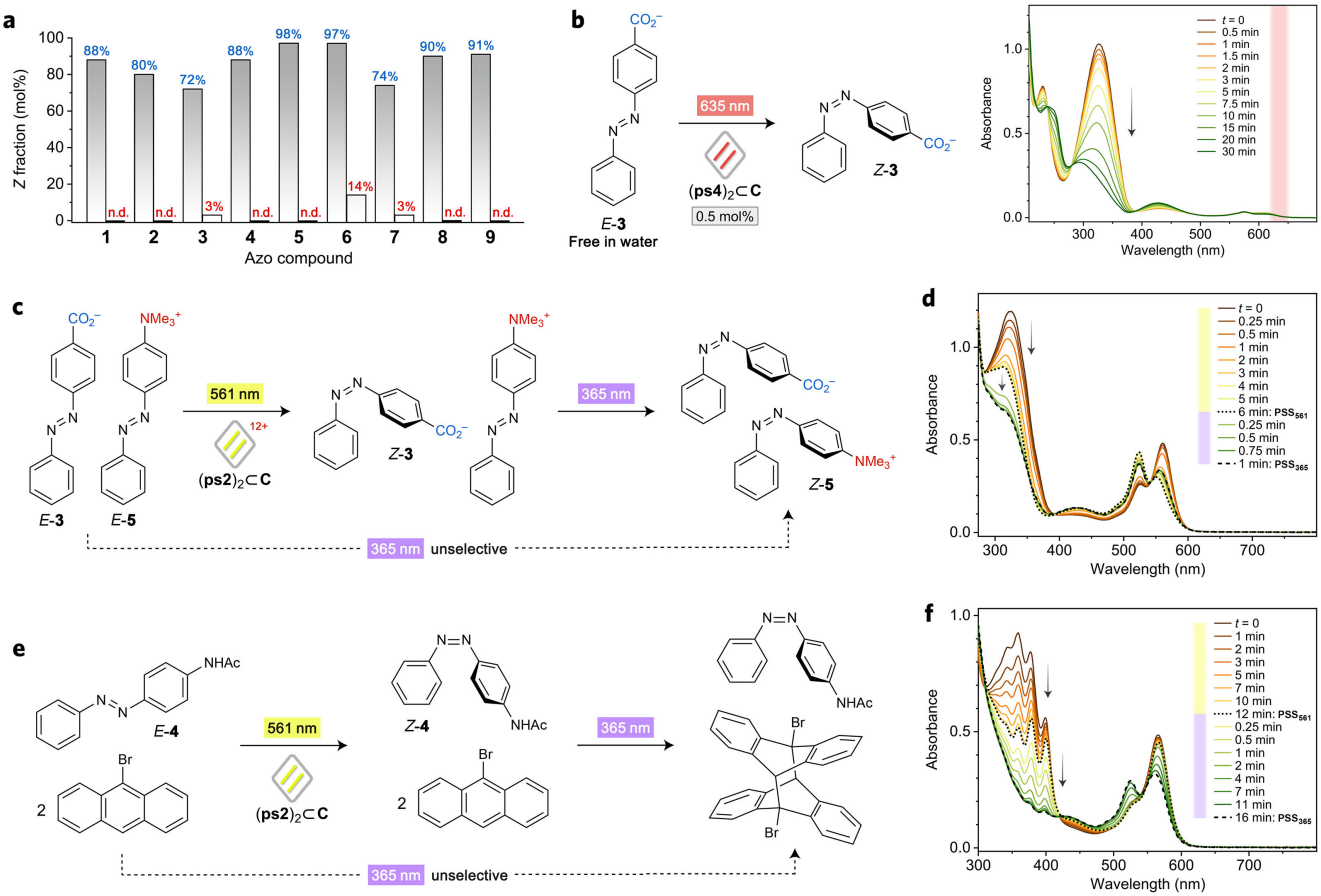

Fig. 5 | Performance of DESC. a, *Blue font:* Composition of the photostationary state (PSS) of azoarenes **1**–**9** subjected to DESC on the millimolar scale in the presence of 0.05 eq of the PS (**ps2** under 561 nm light for **1**–**7**; **ps1** under 525 nm light for **8** and **9**). *Red font:* PSS compositions of the same azoarene/PS mixtures under the same illumination conditions but in the absence of the cage ($CDCl_3$ was used as the solvent, except **3** and **5**, where CD_3OD was used). Illumination times: 15, 12, 35, 12, 40, 24, 45, 4, and 9 min for **1**–**9**, respectively. "n.d." = "not detected" (i.e., the amount of *Z* below the NMR detection limit). **b,** Red-light switching of *E*-**3** dissolved in water in the presence of 0.005 eq. of (**ps4**)$_2$⊂**C** affords a PSS featuring 88% *Z*-**3**. **c,** Selective switching of the negatively charged *E*-**3** with 561 nm light in the presence of the positively charged *E*-**5** on the micromolar scale. **d,** The corresponding absorption spectra. Dotted line: PSS under 561 nm light; dashed line: PSS after the subsequent exposure to 365 nm light (both azobenzenes isomerize to a similar extent). **e,** Selective switching of *E*-**4** with 561 nm light and (**ps2**)$_2$⊂**C** in the presence of a UV-dimerizable anthracene. **f,** The corresponding UV/vis absorption spectra. Dotted line: PSS under 561 nm light; dashed line: after the subsequent exposure to 365 nm light.

To further showcase the potential of DESC, we explored the cavity size and charge (+12) of cage **C** to discriminate between photoreactive compounds whose absorption bands overlap, and which otherwise cannot be converted selectively. To this end, we mixed *E*-**3** and *E*-**5** in a 1:3 ratio and added (**ps2**)$_2$⊂**C** (0.5 eq with respect to **3**; Fig. 5c). At low (micromolar) concentrations, only the negatively charged **3** exhibits a strong affinity to **C**; **5** is not encapsulated owing to the Coulombic repulsion. Indeed, yellow light (561 nm) illumination of this mixture led to a highly selective switching of *E*-**3** (despite the threefold excess of *E*-**5** (Fig. 5d and Supplementary Fig. 99). In

contrast, exposure to UV light induced nonselective switching of both azobenzenes via direct excitation. In the second example, we worked with a mixture of *E*-**4** and 9-bromoanthracene, both in the form of encapsulated homodimers with **C**. Upon exposure to UV light, the encapsulated anthracene rapidly dimerizes to afford the corresponding dianthracene[40] under the same irradiation conditions that trigger the direct *E*→*Z* photoisomerization of **4** (Fig. 5e, right). However, exposing the same mixture to yellow light in the presence of (**ps2**)$_2$⊂**C** induced highly selective photoisomerization of azobenzene, leaving the anthracene intact (Fig. 5f, dotted line). These experiments demonstrate that DESC can be combined with substrate selectivity found in enzymatic systems[56], bringing us closer to realizing the potential of synthetic supramolecular catalysts as "artificial enzymes"[57].

In summary, we described disequilibration by sensitization under confinement (DESC) – a process which, in contrast to traditional azobenzene photosensitization systems, utilizes low-intensity visible light energy to shift the *E*⇄*Z* equilibrium towards the metastable *Z* state. The process is based on a coordination cage with two binding sites, which can be filled by two identical molecules of an *E*-azoarene, a pair of planar dyes, or an azoarene–dye heterodimer. In the latter scenario, the *E*-azoarene is brought in close proximity to the dye and can be sensitized with low-energy visible light of wavelength depending on the identity of the co-confined dye "antenna". As the sensitizers, we used commercially available and inexpensive dyes, which the confinement effect turns into potent triplet sensitizers. The sensitization is followed by azobenzene isomerization to the *Z* isomer, to which the cage has low affinity, expelling it in the presence of additional copies of *E*. On a conceptual level, our system acts as a light-driven supramolecular machine that converts light into chemical energy in the form of out-of-equilibrium photostationary states, some of which contain unprecedented levels of the metastable *Z* isomer (98%) that cannot be obtained by direct photoisomerization with any wavelength of light. DESC is a robust process that works with minute amounts of the caged sensitizers, under ambient conditions (no oxygen exclusion necessary), and for a wide range of aromatic and heterocyclic azoarenes. We envision that in the future, the DESC concept will be extended to other classes of photochromic molecules and, more broadly, will become a powerful tool to control chemical reactivity through a combination of light irradiation and confinement.

Acknowledgments. We acknowledge funding from the European Union's Horizon 2020 Research and Innovation Program (under the European Research Council (ERC) grant agreements 820008 and 101045223, and the Marie Skłodowska-Curie grant agreements 812868 and 101022777) and the Academy of Finland (Center of Excellence Programme LIBER, grant agreement 346107; Flagship Programme PREIN, grant agreement 32016; Postdoctoral Researcher, grant agreement 340103). J.R.C. thanks the Zuckerman STEM Leadership Program for its support. M.O. would like to thank the President's PhD Scholarship for funding. M.J.F. would like to thank the EPSRC for an Established Career Fellowship (grant agreement EP/R00188X/1).

References

1. Herbst, J., Heyne, K. & Diller, R. Femtosecond infrared spectroscopy of bacteriorhodopsin chromophore isomerization. *Science* **297**, 822–825 (2002).
2. Nogly, P. et al. Retinal isomerization in bacteriorhodopsin captured by a femtosecond x-ray laser. *Science* **361**, eaat0094 (2018).
3. Bowmaker, J. K. Evolution of vertebrate visual pigments. *Vision Res.* **48**, 2022–2041 (2008).
4. Douglas, R. H. et al. Dragon fish see using chlorophyll. *Nature* **393**, 423–424 (1998).
5. Isayama, T. et al. An accessory chromophore in red vision. *Nature* **443**, 649–649 (2006).
6. Douglas, R. H., Genner, M. J., Hudson, A. G., Partridge, J. C. & Wagner, H.-J. Localisation and origin of the bacteriochlorophyll-derived photosensitizer in the retina of the deep-sea dragon fish *Malacosteus niger*. *Sci. Rep.* **6**, 12 (2016).
7. Valentini, A., Nucci, M., Frutos, L. M. & Marazzi, M. Photosensitized retinal isomerization in rhodopsin mediated by a triplet state. *ChemPhotoChem* **3**, 925–932 (2019).

8. Bandara, H. M. D. & Burdette, S. C. Photoisomerization in different classes of azobenzene. *Chem. Soc. Rev.* **41**, 1809–1825 (2012).
9. Jerca, F. A., Jerca, V. V. & Hoogenboom, R. Advances and opportunities in the exciting world of azobenzenes. *Nat. Rev. Chem.* **6**, 51–69 (2022).
10. Fischer, E. & Hirshberg, Y. Formation of coloured form of spirans by low-temperature irradiation. *J. Chem. Soc.* **11**, 4522–4524 (1952).
11. Klajn, R. Spiropyran-based dynamic materials. *Chem. Soc. Rev.* **43**, 148–184 (2014).
12. Samanta, D., Mukherjee, S., Patil, Y. P. & Mukherjee, P. S. Self-assembled Pd_6 open cage with triimidazole walls and the use of its confined nanospace for catalytic Knoevenagel- and Diels–Alder reactions in aqueous medium. *Chem. Eur. J.* **18**, 12322–12329 (2012).
13. Mitscherlich, E. Ueber das Stickstoffbenzid. *Ann. Pharm.* **12**, 311–314 (1834).
14. Hartley, G. S. The *cis*-form of azobenzene. *Nature* **140**, 281 (1937).
15. Mativetsky, J. M. et al. Azobenzenes as light-controlled molecular electronic switches in nanoscale metal-molecule-metal junctions. *J. Am. Chem. Soc.* **130**, 9192–9193 (2008).
16. Wang, Z. et al. Storing energy with molecular photoisomers. *Joule* **5**, 3116–3136 (2021).
17. Le, M. & Han, G. G. D. Stimuli-responsive organic phase change materials: Molecular designs and applications in energy storage. *Acc. Mater. Res.* **3**, 634–643 (2022).
18. Klajn, R., Wesson, P. J., Bishop, K. J. M. & Grzybowski, B. A. Writing self-erasing images using metastable nanoparticle “inks". *Angew. Chem. Int. Ed.* **48**, 7035–7039 (2009).
19. Stoll, R. S. & Hecht, S. Artificial light-gated catalyst systems. *Angew. Chem. Int. Ed.* **49**, 5054–5075 (2010).
20. Wei, Y., Han, S., Kim, J., Soh, S. & Grzybowski, B. A. Photoswitchable catalysis mediated by dynamic aggregation of nanoparticles. *J. Am. Chem. Soc.* **132**, 11018–11020 (2010).
21. Lu, J., Choi, E., Tamanoi, F. & Zink, J. I. Light-activated nanoimpeller-controlled drug release in cancer cells. *Small* **4**, 421–426 (2008).
22. Tarn, D. et al. A reversible light-operated nanovalve on mesoporous silica nanoparticles. *Nanoscale* **6**, 3335–3343 (2014).
23. Velema, W. A., Szymanski, W. & Feringa, B. L. Photopharmacology: Beyond proof of principle. *J. Am. Chem. Soc.* **136**, 2178–2191 (2014).
24. Hüll, K., Morstein, J. & Trauner, D. *In vivo* photopharmacology. *Chem. Rev.* **118**, 10710–10747 (2018).
25. Beharry, A. A., Sadovski, O. & Woolley, G. A. Azobenzene photoswitching without ultraviolet light. *J. Am. Chem. Soc.* **133**, 19684–19687 (2011).
26. Bléger, D., Schwarz, J., Brouwer, A. M. & Hecht, S. *o*-Fluoroazobenzenes as readily synthesized photoswitches offering nearly quantitative two-way isomerization with visible light. *J. Am. Chem. Soc.* **134**, 20597–20600 (2012).
27. Ahmed, Z., Siiskonen, A., Virkki, M. & Priimagi, A. Controlling azobenzene photoswitching through combined *ortho*-fluorination and -amination. *Chem. Commun.* **53**, 12520–12523 (2017).
28. Strieth-Kalthoff, F., James, M. J., Teders, M., Pitzer, L. & Glorius, F. Energy transfer catalysis mediated by visible light: Principles, applications, directions. *Chem. Soc. Rev.* **47**, 7190–7202 (2018).
29. Jones, L. B. & Hammond, G. S. Mechanisms of photochemical reactions in solution. XXX. Photosensitized isomerization of azobenzene. *J. Am. Chem. Soc.* **87**, 4219–4220 (1965).
30. Fischer, E. Photosensitized isomerization of azobenzene. *J. Am. Chem. Soc.* **90**, 796–797 (1968).
31. Moreno, J., Gerecke, M., Grubert, L., Kovalenko, S. A. & Hecht, S. Sensitized two-NIR-photon $Z \rightarrow E$ isomerization of a visible-light-addressable bistable azobenzene derivative. *Angew. Chem. Int. Ed.* **55**, 1544–1547 (2016).
32. Isokuortti, J. et al. Expanding excitation wavelengths for azobenzene photoswitching into the near-infrared range via endothermic triplet energy transfer. *Chem. Sci.* **12**, 7504–7509 (2021).
33. Kuntze, K. et al. Azobenzene photoswitching with near-infrared light mediated by molecular oxygen. *J. Phys. Chem. B* **125**, 12568–12573 (2021).
34. Bharmoria, P. et al. Far-red triplet sensitized *Z*-to-*E* photoswitching of azobenzene in bioplastics. *Chem. Sci.* **13**, 11904–11911 (2022).
35. Samanta, D. et al. Reversible photoswitching of encapsulated azobenzenes in water. *Proc. Natl. Acad. Sci. U.S.A.* **115**, 9379–9384 (2018).
36. Hanopolskyi, A. I. et al. Reversible switching of arylazopyrazole within a metal–organic cage. *Beilstein J. Org. Chem.* **15**, 2398–2407 (2019).
37. Gemen, J., Ahrens, J., Shimon, L. J. W. & Klajn, R. Modulating the optical properties of BODIPY dyes by noncovalent dimerization within a flexible coordination cage. *J. Am. Chem. Soc.* **142**, 17721–17729 (2020).

38. Yanshyna, O., Białek, M. J., Chashchikhin, O. V. & Klajn, R. Encapsulation within a coordination cage modulates the reactivity of redox-active dyes. *Comm. Chem.* **5**, 44 (2022).
39. Yanshyna, O., Avram, L., Shimon, L. J. W. & Klajn, R. Coexistence of 1:1 and 2:1 inclusion complexes of indigo carmine. *Chem. Commun.* **58**, 3461–3464 (2022).
40. Gemen, J. et al. Ternary host-guest complexes with rapid exchange kinetics and photoswitchable fluorescence. *Chem* **8**, 2362–2379 (2022).
41. Ishitobi, H., Sekkat, Z. & Kawata, S. Ordering of azobenzenes by two-photon isomerization. *J. Chem. Phys.* **125**, 164718 (2006).
42. Lim, C.-K. et al. Plasmon-enhanced two-photon-induced isomerization for highly-localized light-based actuation of inorganic/organic interfaces. *Nanoscale* **8**, 4194–4202 (2016).
43. Crespi, S., Simeth, N. A. & König, B. Heteroaryl azo dyes as molecular photoswitches. *Nat. Rev. Chem.* **3**, 133–146 (2019).
44. Gonzalez, A. et al. Photocontrolled energy storage in azobispyrazoles with exceptionally large light penetration depths. *J. Am. Chem. Soc.* **144**, 19430–19436 (2022).
45. Weston, C. E., Richardson, R. D., Haycock, P. R., White, A. J. P. & Fuchter, M. J. Arylazopyrazoles: Azoheteroarene photoswitches offering quantitative isomerization and long thermal half-lives. *J. Am. Chem. Soc.* **136**, 11878–11881 (2014).
46. Filatov, M. A. Heavy-atom-free BODIPY photosensitizers with intersystem crossing mediated by intramolecular photoinduced electron transfer. *Org. Biomol. Chem.* **18**, 10–27 (2020).
47. Kähärä, I. et al. Phototoxicity of BODIPY in long-term imaging can be reduced by intramolecular motion. *Photochem. Photobiol. Sci.* **21**, 1677–1687 (2022).
48. Sandros, K. & Bäckström, H. L. J. Transfer of triplet state energy in fluid solutions. *Acta Chem. Scand.* **16**, 958–968 (1962).
49. Eng, J. & Penfold, T. J. Understanding and designing thermally activated delayed fluorescence emitters: Beyond the energy gap approximation. *Chem. Rec.* **20**, 831–856 (2020).
50. Mavrommati, S. A. & Skourtis, S. S. Molecular wires for efficient long-distance triplet energy transfer. *J. Phys. Chem. Lett.* **13**, 9679–9687 (2022).
51. Hammes-Schiffer, S. & Benkovic, S. J. Relating protein motion to catalysis. *Annu. Rev. Biochem.* **75**, 519–541 (2006).
52. Choi, S., Bouffard, J. & Kim, Y. Aggregation-induced emission enhancement of a *meso*-trifluoromethyl BODIPY *via* J-aggregation. *Chem. Sci.* **5**, 751–755 (2014).
53. Bieth, J., Vratsanos, S. M., Wasserman, N. & Erlanger, B. F. Photoregulation of biological activity by photochromic reagents. 2. Inhibitors of acetylcholinesterase. *Proc. Natl. Acad. Sci. U.S.A.* **64**, 1103–1106 (1969).
54. Lerch, M. M., Hansen, M. J., van Dam, G. M., Szymanski, W. & Feringa, B. L. Emerging targets in photopharmacology. *Angew. Chem. Int. Ed.* **55**, 10978–10999 (2016).
55. Fischer, E. The calculation of photostationary states in systems AB when only A is known. *J. Phys. Chem.* **71**, 3704–3706 (1967).
56. Tawfik, D. S. Accuracy-rate tradeoffs: How do enzymes meet demands of selectivity and catalytic efficiency? *Curr. Opin. Chem. Biol.* **21**, 73–80 (2014).
57. Breslow, R. & Overman, L. E. An "artificial enzyme" combining a metal catalytic group and a hydrophobic binding cavity. *J. Am. Chem. Soc.* **92**, 1075–1077 (1970).